Global Interactomics Uncovers Extensive Organellar Targeting by Zika Virus*[S]

Etienne Coyaud‡, Charlene Ranadheera§, Derrick Cheng¶‖, João Gonçalves**, Boris J. A. Dyakov**‡‡, Estelle M. N. Laurent‡, Jonathan St-Germain‡, Laurence Pelletier**‡‡, Anne-Claude Gingras**‡‡, John H. Brumell¶‡‡§§¶¶, Peter K. Kim¶‖, David Safronetz§, and Brian Raught‡‖‖‡‡‡

Zika virus (ZIKV) is a membrane enveloped Flavivirus with a positive strand RNA genome, transmitted by *Aedes* mosquitoes. The geographical range of ZIKV has dramatically expanded in recent decades resulting in increasing numbers of infected individuals, and the spike in ZIKV infections has been linked to significant increases in both Guillain-Barré syndrome and microcephaly. Although a large number of host proteins have been physically and/or functionally linked to other Flaviviruses, very little is known about the virus-host protein interactions established by ZIKV. Here we map host cell protein interaction profiles for each of the ten polypeptides encoded in the ZIKV genome, generating a protein topology network comprising 3033 interactions among 1224 unique human polypeptides. The interactome is enriched in proteins with roles in polypeptide processing and quality control, vesicle trafficking, RNA processing and lipid metabolism. >60% of the network components have been previously implicated in other types of viral infections; the remaining interactors comprise hundreds of new putative ZIKV functional partners. Mining this rich data set, we highlight several examples of how ZIKV may usurp or disrupt the function of host cell organelles, and uncover an important role for peroxisomes in ZIKV infection. ***Molecular & Cellular Proteomics 17: 2242–2255, 2018. DOI: 10.1074/mcp.TIR118.000800.***

Zika virus (ZIKV)[1] is a mosquito-borne (*Aedes aegypti* and *Ae. Albopictus*) single-stranded positive sense RNA arbovirus of the *Flaviviridae* family (1, 2). Named after its discovery in the Zika forest of Uganda in 1947 (3), ZIKV remained confined to Africa until recent outbreaks in Micronesia (2007) (4), French Polynesia (2013) (5), and South America (2015–2016) (6, 7). Local transmission of ZIKV has now been reported in >50 countries (8).

Most ZIKV infections are asymptomatic, though ~20% of infected individuals develop flu-like symptoms (rash, fever, joint pain) that resolve after a few days. Notably, however, ZIKV can infect human neural progenitors and post-mitotic neurons (9, 10). Consistent with these observations, recent ZIKV outbreaks have been linked to significant increases in Guillain-Barré syndrome ((11) an autoimmune disorder affecting neuromuscular function) and microcephaly (12–15), leading the WHO to declare a Public Health Emergency of International Concern. To date, no antiviral drugs or vaccines are available for the treatment or prevention of ZIKV infection.

Phosphatidylserine receptors of the TIM (T-cell immunoglobulin and mucin domain) and TAM (TYRO, AXL, MER) families are candidate ZIKV receptors (16, 17). Following receptor binding, virus endocytosis and vesicle acidification, the 10.7 kb RNA genome is released into the host cell cytoplasm. A single polyprotein is translated from this RNA, then proteolytically cleaved into three structural (Capsid: C; precursor membrane protein: PreM; Env: Envelope) and seven nonstructural (NS) polypeptides (NS1, 2A, 2B, 3, 4A, 4B, and 5) (18, 19). Viral particle assembly occurs in the endoplasmic reticulum, following a dramatic reorganization of host endomembranes (reviewed in (20)).

sh/siRNA and CRISPR-Cas9-based screens have identified several host factors required for ZIKV infection and replication (21–23). Importantly, however, very little is known regarding individual ZIKV protein - host protein interactions. Here, we present a BioID/IP-MS ZIKV-host interactome. Overall, the interactome is significantly enriched in proteins associated with polypeptide processing and quality control, vesicle trafficking, RNA processing machinery and proteins linked to lipid

From the ‡Princess Margaret Cancer Centre, University Health Network, Toronto, Ontario, Canada; §Public Health Agency of Canada, Zoonotic Diseases and Special Pathogens Program, Winnipeg, Manitoba, Canada; ¶Cell Biology Program, Hospital for Sick Children, Toronto, Ontario, Canada; ‖Department of Biochemistry, University of Toronto, Toronto, Ontario, Canada; **Centre for Systems Biology, Lunenfeld-Tanenbaum Research Institute, Sinai Health System, Toronto, Ontario, Canada; ‡‡Department of Molecular Genetics, University of Toronto, Toronto, Ontario, Canada; §§Institute of Medical Science, University of Toronto, Toronto, Ontario, Canada; ¶¶Sick Kids IBD Centre, Hospital for Sick Children, Toronto, Ontario, Canada; ‖‖Department of Medical Biophysics, University of Toronto, Toronto, Ontario M5G 1L7, Canada

Received April 26, 2018, and in revised form, July 6, 2018
Published, MCP Papers in Press, July 23, 2018, DOI 10.1074/mcp.TIR118.000800

metabolism. Notably, the data set also highlights extensive organellar targeting by ZIKV proteins. For example, we report that: (1) the ZIKV Capsid protein is targeted to a variety of host endomembrane locations and can "remodel" nuclear/ER membranes; (2) the NS5 helicase protein is targeted to, and partially disrupts, Cajal Bodies; (3) the NS3-NS2B protease interacts with the HOPS/CORVET complex, and modifies lysosome volume, and; (4) NS2A is specifically targeted to peroxisomal membranes. Consistent with this observation, we demonstrate that peroxisome function is linked to efficient ZIKV replication in culture. Together, the ZIKV-host interactome thus provides a valuable resource for better understanding ZIKV biology and identifies numerous virus-host protein interactions that could be targeted in antiviral therapeutic strategies.

EXPERIMENTAL PROCEDURES

Experimental Design and Statistical Rationale—Both BioID and anti-Flag IP-MS analyses were performed on each of the ten ZIKV polypeptides, expressed individually in HEK293 T-REx cells, fused either with an N-terminal FlagBirA* or a C-terminal BirA*Flag epitope tag. MS samples prepared from two biological replicates were each analyzed twice (*i.e.* four MS runs) on a Thermo Q-Exactive HF quadrupole-Orbitrap mass spectrometer. For each prey protein, all four sample runs were compared against the two highest peptide counts among 16 control samples, prepared from HEK293 T-REx cells expressing the FlagBirA* tag alone (see below). Protein IDs with at least two unique peptides and an iProphet score >0.9 (corresponding to ~1% FDR) were defined as high-confidence interactors, when their Bayesian False Discovery Rate (BFDR) assigned by SAINT Express (v3.6) was below 1% (supplemental Table S1). Additional details provided below.

Cell Lines, Virus, and Transfection—Individual ZIKV polypeptide sequences were generated by gene synthesis (BioBasics, Markham, ON, Canada; based on Genbank sequence ANO46305.1, and cleavage sites reported in (18); full sequence information available on Prohits-web.lunenfeld.ca), and subcloned using AscI/NotI sites into pcDNA5.1 FRT/TO FlagBirA*- (N-terminal tagging), FRT/TO -BirA*Flag (C-terminal tagging), pcDNA3 GFP-, or pcDNA3 mCherry-plasmids. FAM134B was amplified with Q5 polymerase (NEB, Ipswich, MA) from HEK293 cDNA, with the following primers: KpnI-Fwd: TATAGGTACCATGGCGAGCCCGGCGCCTCCGG and AscI_Rev AAGGCGCGCCTTACTTGTCGTCATCGTCTTTGTAGTCGGCATGGCCTCCCAGCA GATTTG, and inserted into pcDNA3. Epitope-tagged ZIKV coding vectors were transfected with PolyJet (Signagen, Rockville, MD), and expressed in human Flp-In T-REx 293 cells (Invitrogen, Carlsbad, CA) or HeLa cells (as described in (24)). Protein expression was induced by adding 1 μg/ml tetracycline to the culture medium (DMEM, 10% fetal calf serum, Gibco, Waltham, MA) for 24 h. 293 T-REx cells were maintained at 37 °C in DMEM supplemented with 10% fetal bovine serum, 10 mM HEPES (pH 8.0) and 1% penicillin-streptomycin. HeLa cells were cultured under the same conditions. Human fibroblasts were cultured in DMEM with L-glutamine (Wisent, St-Bruno, QC, Canada) supplemented with 10% fetal bovine serum (Gibco) at 37 °C in humidified air with 5% CO_2. Vero cells were cultured in MEM with L-glutamine supplemented with 5% fetal bovine serum at 37 °C and 5% CO_2. ZIKV (ZIKV/Homo sapiens/PRI/PRVABC59/2015, Genbank accession no. KX087101.2) was amplified in Vero cells using MEM supplemented with L-glutamine and 1% fetal bovine serum. Plasmids were transfected using Lipofectamine-2000 (Invitrogen) following the manufacturer's instructions.

Zika Virus Infection—Cells at 70% confluence were rinsed with PBS, and virus diluted in growth medium supplemented with L-glutamine and 1% FBS. Virus inoculum was removed after 1 h and replaced with fresh media. Cells and supernatants were harvested at the indicated times post-infection for determination of $TCID_{50}$.

Flag Affinity Purification—5 × 150 cm^2 dishes of subconfluent (80%) 293 T-REx cells expressing the protein of interest were scraped into PBS, pooled, washed twice in 10 ml PBS, and collected by centrifugation at 1000 × *g* for 5 min at 4 °C. Cell pellets were stored at −80 °C until lysis. The cell pellet was weighed, and 1:4 pellet weight/lysis buffer (by volume) was added. Lysis buffer consisted of 50 mM HEPES-NaOH (pH 8.0), 100 mM KCl, 2 mM EDTA, 0.1% Nonidet P-40, 10% glycerol, 1 mM PMSF, 1 mM DTT, and 1:500 protease inhibitor mixture (Sigma-Aldrich, St. Louis, MO). On resuspension, cells were incubated on ice for 10 min, subjected to one additional freeze-thaw cycle, then centrifuged at 27,000 × *g* for 20 min at 4 °C. The supernatant was transferred to a fresh 15 ml conical tube, and 1:1000 turbonuclease (BioVision, Milpitas, CA) plus 30 μl packed, pre-equilibrated Flag-M2 agarose beads (Sigma-Aldrich) were added. The mixture was incubated for 2 h at 4 °C with end-over-end rotation. Beads were pelleted by centrifugation at 1000 × *g* for 1 min and transferred with 1 ml of lysis buffer to a fresh centrifuge tube. Beads were washed once with 1 ml lysis buffer and twice with 1 ml ammonium bicarbonate (ammbic) rinsing buffer (50 mM ammbic, pH 8.0, 75 mM KCl). Elution was performed by incubating the beads with 150 μl of 125 mM ammonium hydroxide (pH ~11). The elution step was repeated twice, and the combined eluate centrifuged at 15,000 × *g* for 1 min, transferred to a fresh centrifuge tube, and lyophilized.

Biotin-streptavidin Affinity Purification—Cell pellets were resuspended in 10 ml of lysis buffer (50 mM Tris-HCl pH 7.5, 150 mM NaCl, 1 mM EDTA, 1 mM EGTA, 1% Triton X-100, 0.1% SDS, 1:500 protease inhibitor mixture (Sigma-Aldrich), 1:1000 turbonuclease), incubated on an end-over-end rotator at 4 °C for 1 h, briefly sonicated to disrupt any visible aggregates, then centrifuged at 16,000 × *g* for 30 min at 4 °C. The supernatant was transferred to a fresh 15 ml conical tube, 30 μl of packed, pre-equilibrated streptavidin-Sepharose beads (GE, Boston, MA) were added, and the mixture incubated for 3 h at 4 °C with end-over-end rotation. Beads were pelleted by centrifugation at 2000 rpm for 2 min and transferred with 1 ml of lysis buffer to a fresh Eppendorf tube. Beads were washed once with 1 ml lysis buffer and twice with 1 ml of 50 mM ammbic (pH 8.3). Beads were transferred in ammbic to a fresh centrifuge tube and washed two more times with 1 ml ammbic buffer. Tryptic digestion was performed by incubating the beads with 1 μg MS grade TPCK trypsin (Promega, Madison, WI) dissolved in 200 μl of 50 mM ammbic (pH 8.3) overnight at 37 °C. The following morning, an additional 0.5 μg trypsin was added, and the beads incubated for 2 h at 37 °C. Beads were pelleted by centrifugation at 2000 × *g* for 2 min, and the supernatant was transferred to a fresh Eppendorf tube. Beads were washed twice with 150 μl of 50 mM ammonium bicarbonate, and washes pooled with the eluate. The sample was lyophilized and resuspended in buffer A (0.1% formic acid). One-fifth of the sample was analyzed per MS run.

Mass Spectrometry Analysis—High performance liquid chromatography was conducted using a 2 cm pre-column (Acclaim PepMap 50 mm × 100 μm inner diameter (ID)) and 50 cm analytical column (Acclaim PepMap, 500 mm × 75 μm ID; C18; 2 um; 100 Å, Thermo

[1] The abbreviations used are: ZIKV, Zika virus; BioID, proximity-dependent biotin identification; CB, Cajal body; CRISPR, clustered regularly interspersed short palindromic repeats; C, capsid protein; DENV, Dengue virus; Env, ZIKV envelope protein; GO, gene ontology; IF, immunofluorescence; NS1–5, ZIKV nonstructural viral proteins 1–5; PreM, ZIKV pre-membrane/membrane protein; sh/siRNA, short hairpin/small interfering RNA; UPS, ubiquitin-proteasome system.

Fisher Scientific, Waltham, MA), running a 120 min reversed-phase buffer gradient at 225 nl/min on a Proxeon EASY-nLC 1000 pump in-line with a Thermo Q-Exactive HF quadrupole-Orbitrap mass spectrometer. A parent ion scan was performed using a resolving power of 60,000, then up to the twenty most intense peaks were selected for MS/MS (minimum ion count of 1000 for activation) using higher energy collision induced dissociation (HCD) fragmentation. Dynamic exclusion was activated such that MS/MS of the same *m/z* (within a range of 10 ppm; exclusion list size = 500) detected twice within 5 s were excluded from analysis for 15 s. For protein identification, Thermo .RAW files were converted to the .mzXML format using ProteoWizard (v3.0.10800; 4/27/2017) (25). Using the Trans-Proteomic Pipeline (TPP v4.7 Polar Vortex rev 1, linux build 201705011551) converted files were searched using X!Tandem (Jackhammer TPP 2013.06.15.1) (26) and Comet (2014.02 rev. 2) (27) against the Human RefSeq Version 45 database (containing 36113 entries). Search parameters specified a parent ion mass tolerance of 10 ppm, and an MS/MS fragment ion tolerance of 0.4 Da, with up to 2 missed cleavages allowed for trypsin. No fixed modifications were used. Variable modifications of +16@M and W, +32@M and W, +42@N terminus, and +1@N and Q were allowed. Proteins identified with an iProphet cut-off of 0.9 (corresponding to ≤1% FDR) and at least two unique peptides were analyzed with SAINT Express v.3.6. Control runs (16 runs for BioID; 16 runs for IP-MS; all from cells expressing the FlagBirA* epitope tag only) were collapsed to the four highest spectral counts for each prey, and high confidence interactors were defined as those with BFDR≤0.01. Each bait protein was analyzed with both an N- and C-terminal BirA* tag. Two biological replicates (*i.e.* separate transfections) were each subjected to two MS runs (two technical replicates). Each of the ten ZIKV bait proteins was analyzed using both BioID and Flag IP, for a total of 160 MS runs. Average R^2 between technical replicates: 0.976. Average R^2 between biological replicates: 0.888 (supplemental Table S1).

Networks and Clustering Analysis—SAINT data were imported into Cytoscape 3.4 (http://www.cytoscape.org). All network files and parameters are available at http://prohits-web.lunenfeld.ca/.

Immunofluorescence, Image Acquisition, and Processing—Transiently transfected HeLa cells expressing GFP- or FlagBirA*-tagged proteins were grown on coverslips, fixed with 4% paraformaldehyde for 15 min, and washed in PBS with 0.1% Triton X-100. Cells were blocked in 5% bovine serum albumin (BSA) in PBS for 30 min before incubating in the indicated primary antibodies for 1 h at RT. Primary antibodies were used at the following concentrations: anti-FLAG M2 (1:500; Sigma-Aldrich), anti-CANX C5C9 (1:50; Cell Signaling Technologies, Danvers, MA), anti-Lamin B1 (1:1000; Abcam 16048), anti-COIL (1:1000; Abcam 11822), anti-P4HB (1:1000; Stressgen, Victoria, BC, Canada, SPA-891), anti-Fibrillarin (1:100; Abcam 5821). After removing the antibody solution, cells were washed once and incubated for 1 h with anti-mouse or anti-rabbit Alexa (488, 594, or 647)-conjugated secondary antibodies. In some cases, Streptavidin-Alexa594 (1:5000, Invitrogen) or BODIPY 493/503 (1:100, Invitrogen) were added with secondary antibodies. Cells were washed twice with PBS, then with 1 μg/ml of 4′,6-diamidino-2- phenylindole (DAPI) in PBS for 5 min. After washing with PBS three more times for 5 min each, coverslips were mounted with ProLong Gold Antifade (Thermo Fischer Scientific). Cells were imaged using PlanApo 60X oil lens, NA 1.40 on an Olympus FV1000 confocal microscope (zoom factor between 3–5; Olympus America, Melville, NY). Images were processed using the Volocity Viewer v.6 and assembled using Adobe Illustrator CS6 (Adobe Systems Inc.).

Cajal Body Quantification—HeLa cells were transfected with the FlagBirA*-NS5 vector, incubated 24 h, then incubated an additional 24 h on coverslips with biotin (50 μM). Cells were fixed and permeabilized as above, then stained with anti-COIL and Streptavidin AF594 (as a reporter of positive FlagBirA*-NS5 cells). Cajal body (CB) volumes (red objects gated between 0.1–5 μm^3) were quantified using the Volocity 6.0 measurement tool. In each experiment, CB volumes (COIL-positive nuclear bodies) were quantified in DAPI positive objects (gated between 100–500 μm^3) of the NS5-positive gated population *versus* the NS5 low/negative gated population. Data (raw data supplemental Table S4) of 25 stitched fields for each of the two independent experiments were merged and plotted using Excel. For calculation of the number of CB/cell, three nonoverlapping fields per experiment were used, and the number of CB observed in each subpopulation was averaged according to the number of nuclei (supplemental Table S3). Student's *t* test was performed with Excel T.TEST function (Microsoft, Redmond, WA).

Lysosome Quantification—HeLa cells were transfected with the indicated GFP-tagged constructs and incubated 48 h on coverslips at 37 °C. Cultured cells were stained with 1 μg/ml of Hoechst 33342 dye (Fisher Scientific) for 15 min at 37 °C. Cells were washed twice with pre-warmed PBS, before incubating in DMEM with no pH indicator (GIBCO, Invitrogen). Lysotracker Red DND-99 (Molecular Probes, Eugene, OR) was used at 50 nM for 30 min. Coverslips were fixed with 4% paraformaldehyde for 15 min, then washed three times with PBS, and mounted. Lysosome volumes (red objects gated between 0.1–5 μm^3) were quantified using the Volocity 6.0 measurement tool. Data from 16 stitched fields per condition were merged. ANOVA was performed with the FUNCRES.XLAM Excel add-in. Student's *t* test was performed with Excel T.TEST function (Microsoft). Graph and data distribution were assembled with Excel.

Centriolar Satellite Microscopy—Cells were probed with a PCM1 rabbit polyclonal antibody (A301–149A, Bethyl, Montgomery, TX) and imaged with a 60× oil-immersion objective (1.42 NA) on a Deltavision Elite DV imaging system equipped with sCMOS 2048 × 2048 pixels2 camera (GE Healthcare). Z stacks (0.2 um) were collected, deconvolved using softWoRx v5.0 (Applied Precision, Mississauga, ON, Canada) and are shown as maximum intensity projections (pixel size 0.1064 um).

Peroxisome Microscopy—Cells were fixed in paraformaldehyde and permeabilized with 0.1% Triton X-100 in PBS, followed by incubation with the indicated antibodies. A Zeiss LSM 710 laser-scanning confocal microscope with a 63 × 1.4 NA oil immersion objective was used to acquire fluorescence images of cells. Z-stacks series were collected for measuring cell and peroxisome volume. Volocity 5.0 software (Perkin Elmer, Waltham, MA) was used to quantify cell volume, peroxisome number (peroxisome density) and peroxisome volume. ImageJ (NIH, Bethesda) was used to adjust brightness and contrast of images.

Immunoblotting and Co-IP—Vero cell lysates in Laemmli buffer were analyzed by SDS-PAGE and subjected to Western blotting using: rabbit monoclonal anti-PMP70 (Abcam, Cambridge, UK), rabbit polyclonal anti-PEX14 (Millipore, Burlington, MA), mouse monoclonal anti-ATP5A (Abcam), mouse monoclonal anti-GAPDH-HRP (Novusbio, Littleton, CO), goat anti-rabbit IgG-HRP (Santa Cruz, Dallas, TX), goat anti-mouse IgG-HRP (Cedarlane, Burlington, ON, Canada). FlagBirA*-tagged protein extression was assayed by SDS-PAGE and Western blotting using: anti-FLAG M2, and biotinylated substrates visualized with Streptactin-HRP (BioRad, Hercules, CA, 1:10000 in PBS 0.1% Tween, 5% BSA). Co-IP was performed on 293 T-REx cells expressing FlagBirA*-NS3, as described in (4) and proteins analyzed by SDS-PAGE and Western blotting using anti-CEP85 antibody (Abnova, Taipei City, Taiwan H00064793-B01P, 1:500).

RESULTS

The ZIKV genome encodes a single large polyprotein, which is cleaved by viral and host cell proteases to generate ten distinct polypeptides (Fig. 1*A*). To better understand ZIKV-

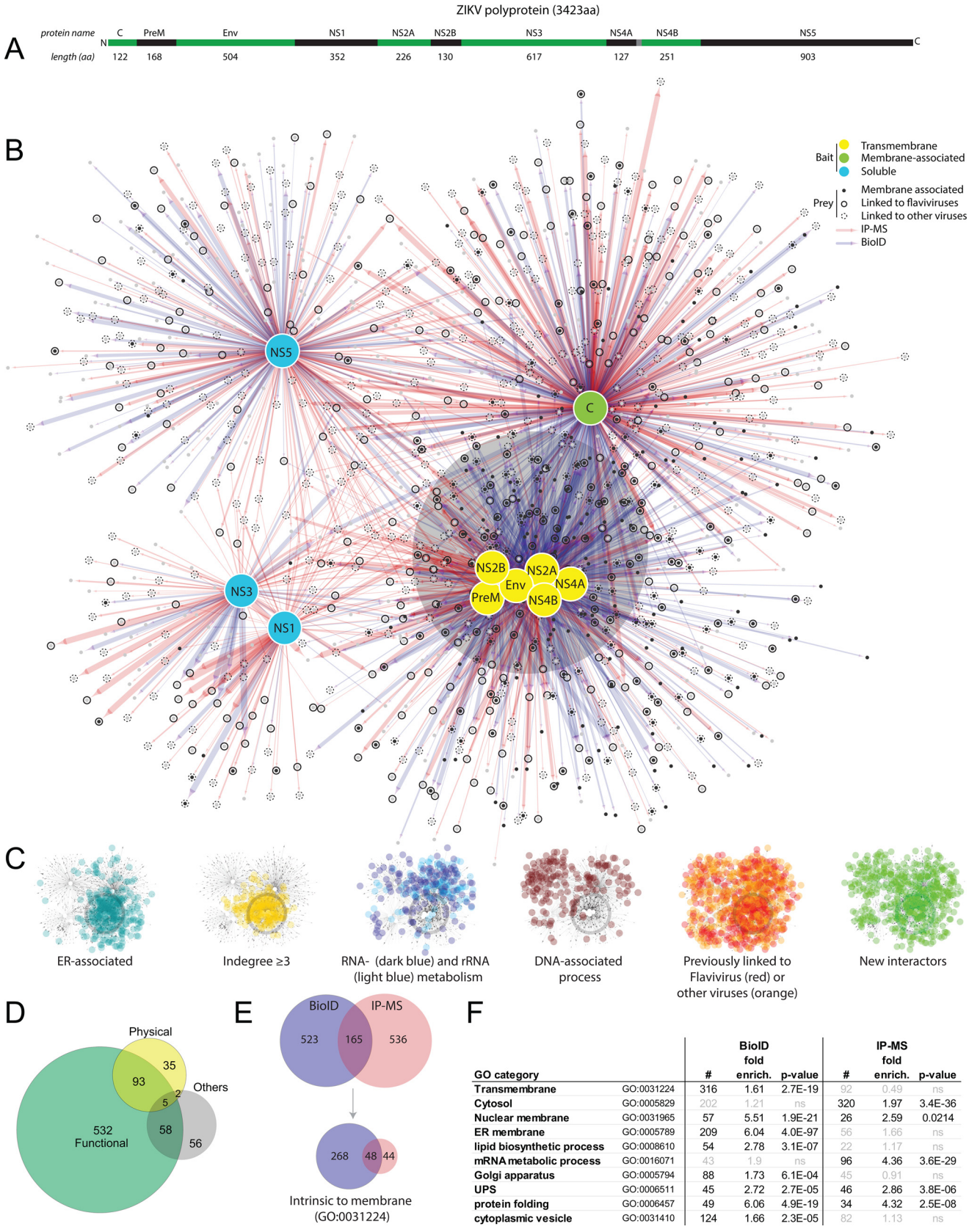

F

GO category		BioID #	BioID fold enrich.	BioID p-value	IP-MS #	IP-MS fold enrich.	IP-MS p-value
Transmembrane	GO:0031224	316	1.61	2.7E-19	92	0.49	ns
Cytosol	GO:0005829	202	1.21	ns	320	1.97	3.4E-36
Nuclear membrane	GO:0031965	57	5.51	1.9E-21	26	2.59	0.0214
ER membrane	GO:0005789	209	6.04	4.0E-97	56	1.66	ns
lipid biosynthetic process	GO:0008610	54	2.78	3.1E-07	22	1.17	ns
mRNA metabolic process	GO:0016071	43	1.9	ns	96	4.36	3.6E-29
Golgi apparatus	GO:0005794	88	1.73	6.1E-04	45	0.91	ns
UPS	GO:0006511	45	2.72	2.7E-05	46	2.86	3.8E-06
protein folding	GO:0006457	49	6.06	4.9E-19	34	4.32	2.5E-08
cytoplasmic vesicle	GO:0031410	124	1.66	2.3E-05	82	1.13	ns

host interactions, the ten ZIKV proteins were fused in-frame with an N- or C-terminal Flag-BirA R118G tag (constructs based on ZIKV H/PF/2013 ANO46305.1 (28); individual proteins based on cleavage sites reported in (18)) and expressed in HEK 293 cells, a system that displays characteristics of immature neurons (29) and which can be infected with ZIKV (30) (supplemental Fig. S1*A*, S1*B*). Bait protein localization was queried using anti-Flag immunofluorescence (IF) confocal microscopy (supplemental Fig. S1*C*; additional IF available at ProHits-web.ca). Localizations were consistent with several previous reports on ZIKV and/or related Flaviviral proteins (supplemental Fig. S1*C*). Colocalization of otherwise identical N- and C-terminal-tagged ZIKV proteins indicated that the tagging moieties did not significantly affect intracellular localization (supplemental Fig. S1*D*).

Using these cells, the virus-host protein interaction landscape was characterized using immunoprecipitation coupled with mass spectrometry (Flag IP-MS) and proximity-dependent biotin identification (BioID (31), supplemental Table S1, supplemental Fig. S2*A*–S2*B*; searchable data set available at ProHits-web.ca; raw data available at massive.ucsd.edu, accession #MSV000082311). Using a Bayesian false discovery rate of ≤1%, 3033 high confidence interactions were identified among 1224 unique human proteins.

To better understand the ZIKV-host interactome, a self-organized force-directed bait-prey topology map was generated, in which map location is determined by the number and abundance (*i.e.* total peptide counts) of host interactors (Fig. 1*B*). As expected, this approach closely clustered all six predicted ZIKV transmembrane proteins. This "core" map region encompasses the most highly interconnected preys (*i.e.* those that interact with the highest number of baits; Fig. 1*C*) and is enriched for nuclear, endoplasmic reticulum (ER), Golgi and other membrane polypeptides. Capsid protein (C) interactors were enriched in both membrane and nonmembrane proteins; this bait polypeptide thus occupies a distinct territory connected to, yet slightly removed from, the core. The three nonmembrane ZIKV proteins (NS1, NS3, and NS5) occupy peripheral areas of the map (Fig. 1*B*). These areas are enriched for *e.g.* DNA and RNA-associated proteins (Fig. 1*C*). Previously described virus protein interactors and putative novel interactors are represented throughout the map (Fig. 1*C*).

Three hundred forty-seven physical or functional interactors previously implicated in Flavivirus infection, and an additional 434 interactors linked to other viruses, are represented in the ZIKV interactome (Fig. 1*D*; supplemental Table S1), comprising >60% of the interaction network and highlighting the quality of the data set. 738 polypeptides were detected as high confidence interactors for a single ZIKV bait protein, revealing a high degree of specificity for the viral-host interactions. Relevant to the link between ZIKV infection and fetal brain development, more than 85% of the ZIKV interacting proteins identified in HEK 293 cells are expressed in the human cerebral cortex (32) (supplemental Fig. S2*C*, supplemental Table S2).

One hundred sixty-five proteins were detected by both BioID and IP-MS (Fig. 1*E*). This protein population was significantly enriched for host components localized to soluble cellular fractions (*e.g.* RNA binding proteins (73/165; GO:0003723) and nucleolar (54/165; GO:0005730) components) but was depleted for membrane proteins (supplemental Table S2). Only ten interactors in this group were annotated as intrinsic to intracellular membranes (GO:0031300).

Although the two techniques identified a roughly equal number of high confidence interactors (701 *versus* 688 proteins identified by IP-MS and BioID, respectively), BioID identified >3x more membrane-associated polypeptides (Fig. 1*E*; see supplemental Table S3 for all GO annotations). Consistent with this observation, although both data sets are enriched for *e.g.* ubiquitin proteasome system (UPS) components, the IP-MS data set is uniquely enriched in cytoplasmic polypeptides and RNA processing proteins, whereas the BioID data set is specifically enriched for nuclear, ER and Golgi membrane proteins, cytoplasmic vesicle and lipid droplet components (Fig. 1*F*). Like previous reports (33, 34), our data thus suggest that IP-MS and BioID sample largely discrete protein populations and intracellular environments, and thereby identify complementary interactor sets.

Consistent with previous CRISPR- and sh/siRNA-based screens identifying host proteins required for Flavivirus replication (21–23, 35, 36), multiple ZIKV polypeptides interact with components of the ER signal peptidase complex, ER membrane complex, glucosyltransferases and the BAT3 tail-anchored membrane protein insertion complex (Fig. 2*A*). This large suite of host proteins is thus likely to be required for proper ZIKV polypeptide folding, processing, post-translational modification, membrane localization and virion assembly.

FIG. 1. **A ZIKV-host protein topology map.** *A*, The Zika virus (ZIKV) polyprotein. Position and individual protein length (in amino acids) are indicated. *B*, Self-organized prefuse force-directed topology map (based on peptide count sum of four mass spectrometry runs) for the ZIKV-host interactome. Bait proteins are represented by larger nodes, interactors represented by smaller nodes. Prey proteins previously physically or functionally linked to Flaviviruses (solid circle) or any other virus (broken circle) are indicated. Edge thickness is proportional to spectral counts. Red edge indicates an interaction detected by IP-MS, blue edge indicates those detected by BioID. *C*, Map positions of the indicated protein groups overlaid on a thumbnail of the topology map. *D*, Venn diagram depicting category breakdown of previously published virus-host interactions; functional interactions (green), physical interactions (yellow) or other (gray). *E*, Number of high confidence interacting partners identified by each method, as indicated (*top*); number of membrane proteins identified by each technique (*bottom*). *F*, Gene ontology category enrichment for BioID and IP-MS data sets. (See supplemental Table S2 for full GO category analysis.)

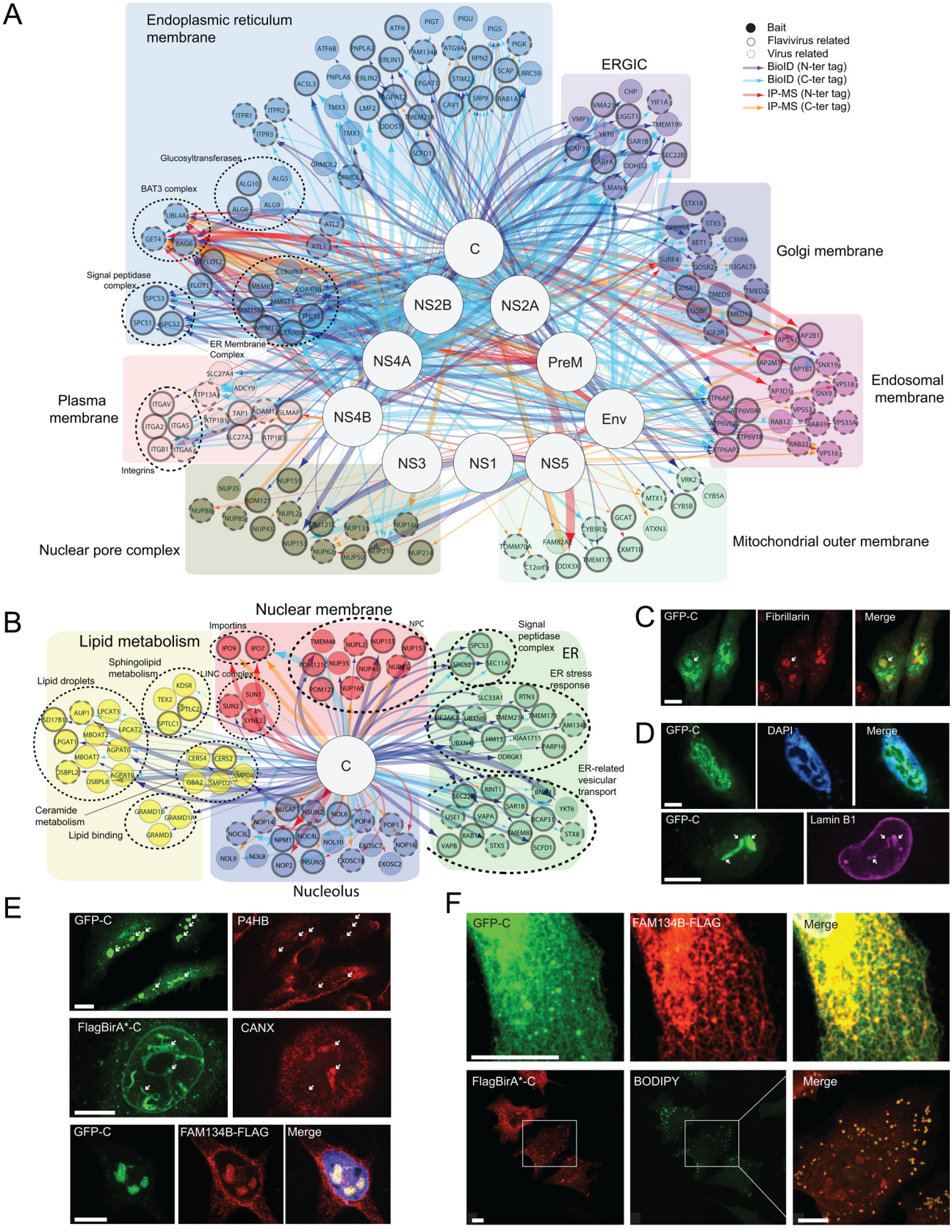
A
Endoplasmic reticulum membrane
ERGIC
Golgi membrane
Endosomal membrane
Plasma membrane
Nuclear pore complex
Mitochondrial outer membrane
Glucosyltransferases
BAT3 complex
Signal peptidase complex
ER Membrane Complex
Integrins
Bait
Flavivirus related
Virus related
BioID (N-ter tag)
BioID (C-ter tag)
IP-MS (N-ter tag)
IP-MS (C-ter tag)
C
NS2B
NS2A
NS4A
PreM
NS4B
Env
NS3
NS1
NS5
B
Nuclear membrane
Lipid metabolism
Importins
NPC
Signal peptidase complex
ER
ER stress response
Sphingolipid metabolism
Lipid droplets
LINC complex
Ceramide metabolism
Lipid binding
ER-related vesicular transport
Nucleolus
C
GFP-C
Fibrillarin
Merge
D
GFP-C
DAPI
Merge
GFP-C
Lamin B1
E
GFP-C
P4HB
FlagBirA*-C
CANX
GFP-C
FAM134B-FLAG
Merge
F
GFP-C
FAM134B-FLAG
Merge
FlagBirA*-C
BODIPY
Merge

Individual ZIKV protein interactomes revealed targeting to host proteins with a variety of biological functions. For example, the Capsid (C) protein IP-MS identified interactions with multiple nucleolar proteins (Fig. 2*B*). Consistent with this observation and previous reports demonstrating that the related Dengue virus (DENV) capsid protein is localized to the nucleolus (37), IF confocal microscopy of ZIKV C-expressing cells revealed colocalization with the nucleolar marker fibrillarin (Fig. 2*C*). BioID identified C proximity interactions at the nuclear, ER and other membranes (Fig. 2*B*). C is also localized to DAPI-poor nuclear structures not associated with fibrillarin, and which are not observed in cells expressing other ZIKV proteins (Fig. 2*D*, supplemental Fig. S1*C*). These structures were also detected by antibodies directed against lamin B1, suggesting that they are derived (at least in part) from the nuclear membrane. Surprisingly, these structures were also detected by antibodies directed against the ER markers prolyl 4-hydroxylase subunit B (P4HB) and calnexin (CANX; Fig. 2*E*). Consistent with this observation, when Flag-FAM134B (a C-interacting protein required for ER-specific autophagy (38) and which inhibits ZIKV replication (39)) was coexpressed with GFP-Capsid protein, it was also recruited to these nuclear structures (Fig. 2*E*). Like other Flaviviruses, ZIKV extensively remodels the host endomembrane system to create viral replication factories (40). Although additional study will be required to better understand these C-associated structures, our observations are consistent with previous reports (*e.g.* (41)) suggesting that ZIKV promotes the inward budding of host membranes.

In the cytoplasm, C is localized to the ER and vesicular structures (Fig. 2*F*). The C interactome includes several proteins associated with lipid storage and metabolism (Fig. 2*B*) and, consistent with previous work demonstrating that both DENV and Hepatitis C virus capsid proteins localize to the surface of lipid droplets (42), cytoplasmic ZIKV C colocalizes with the lipid droplet marker Bodipy 493/503 (Fig. 2*F*). Together, these findings reveal multiple putative roles for C in remodeling host cell membranes and highlight the advantages of using both IP-MS and BioID for a more complete characterization of protein-protein interactions.

The other ZIKV proteins are targeted to a number of additional host cell systems and organelles. For example, consistent with a recent report (43), our Flag IP-MS links ZIKV NS5 to the STAT2 signaling protein (supplemental Table S1) as well as DDA1, DDB1 and VPRBP/DCAF1 (Fig. 3*A*), components of a host cell ubiquitin E3 ligase previously linked to several other viruses (44). IP-MS conducted on both DDB1 and VPRBP/DCAF1 in the presence of NS5 validated these interactions for the ZIKV NS5 protein (Fig. 3*A*, supplemental Table S4).

NS5 BioID also identified components of the Cajal Body (CB; Fig. 3*B*), a nuclear organelle with crucial roles in spliceosomal snRNP maturation (45). The influenza A virus nucleoprotein is also localized to CBs (46) but little is known regarding the role of this organelle in the Flavivirus life cycle. Consistent with our data, both NS5 (but no other ZIKV proteins; Fig. 3*C*, supplemental Fig. S3) and biotinylated proteins in NS5-expressing cells (Fig. 3*D*) colocalize with the CB marker coilin. BioID conducted on coilin in the presence and absence of NS5 (Fig. 3*B*, supplemental Table S5) validated this interaction. Notably, NS5 expression was also uniquely associated with significantly increased numbers of CB/cell, accompanied by a significant decrease in CB volume (Fig. 3*E*, supplemental Table S6). NS5 thus appears to disrupt CBs.

NS3 BioID identified *e.g.* the Vaccinia restriction factor WDR6 (47) and the HIV1 dependence factor HELZ (48) as interacting partners. NS3 IP-MS identified the DENV host factor FASTKD5 (49) and UPS components previously linked to West Nile virus replication (50). NS3 IP-MS also identified VPS33A, VPS18 and VPS16, core components of the HOPS/CORVET vesicle tethering complexes (Fig. 3*F*) required for endosome-lysosome fusion (51). Although no previous link with Flaviviruses has been reported, a genome-wide screen identified the HOPS complex as an Ebola restriction factor (52). Notably, consistent with the NS3-HOPS/CORVET interaction, cells expressing both NS3 and its cofactor NS2B (53) exhibited significantly smaller lysosomes (Fig. 3*G*, supplemental Table S7), suggesting that the NS3-NS2B protease complex could disrupt lysosome function.

ZIKV infection has been linked to significant defects in centrosome function (54, 55). Consistent with these observations, our data reveal ZIKV polypeptide interactions with multiple centrosome and cilia regulatory proteins. For example, NS3 (Fig. 3*H*) interacts with UNC119B, a myristoyl chaperone required for recruiting NPHP (nephronophthisis) proteins to cilia (56); CEP192, a major regulator of centrosome and spindle assembly; OFD1, a centrosome/centriolar satellite protein (57); and CEP85, a protein linked to centrosome biogenesis

FIG. 2. **Individual ZIKV proteins interact with both shared and unique subsets of host proteins linked to a variety of biological functions.** *A*, ZIKV proteins interact extensively with the host endomembrane system. Bait proteins are represented by larger nodes, interactors represented by smaller, color-coded nodes, and grouped according to intracellular localization. Interactions detected by BioID are indicated with blue edges (dark blue detected with N-terminal tagged ZIKV bait protein, light blue detected by C-terminal tagged bait protein); interactions detected by IP-MS are indicated by red and orange edges. Prey proteins previously linked to Flavivirus function are encircled in solid gray, prey previously linked to other viruses are highlighted with a broken gray circle. *B*, C interacts with nucleolar proteins, nuclear and ER membrane proteins, and polypeptide components of lipid droplets. *C*, C colocalizes with the nucleolar marker fibrillarin. Immunofluorescence microscopy of GFP-tagged C protein and endogenous fibrillarin. All scale bars 10 μm. *D*, Nuclear C protein occupies DAPI-poor regions, and colocalizes with the nuclear membrane protein lamin B1. *E*, Nuclear C colocalizes with the ER markers P4HB, CANX and FAM134B. *F*, Cytoplasmic C is localized to the ER and lipid droplets.

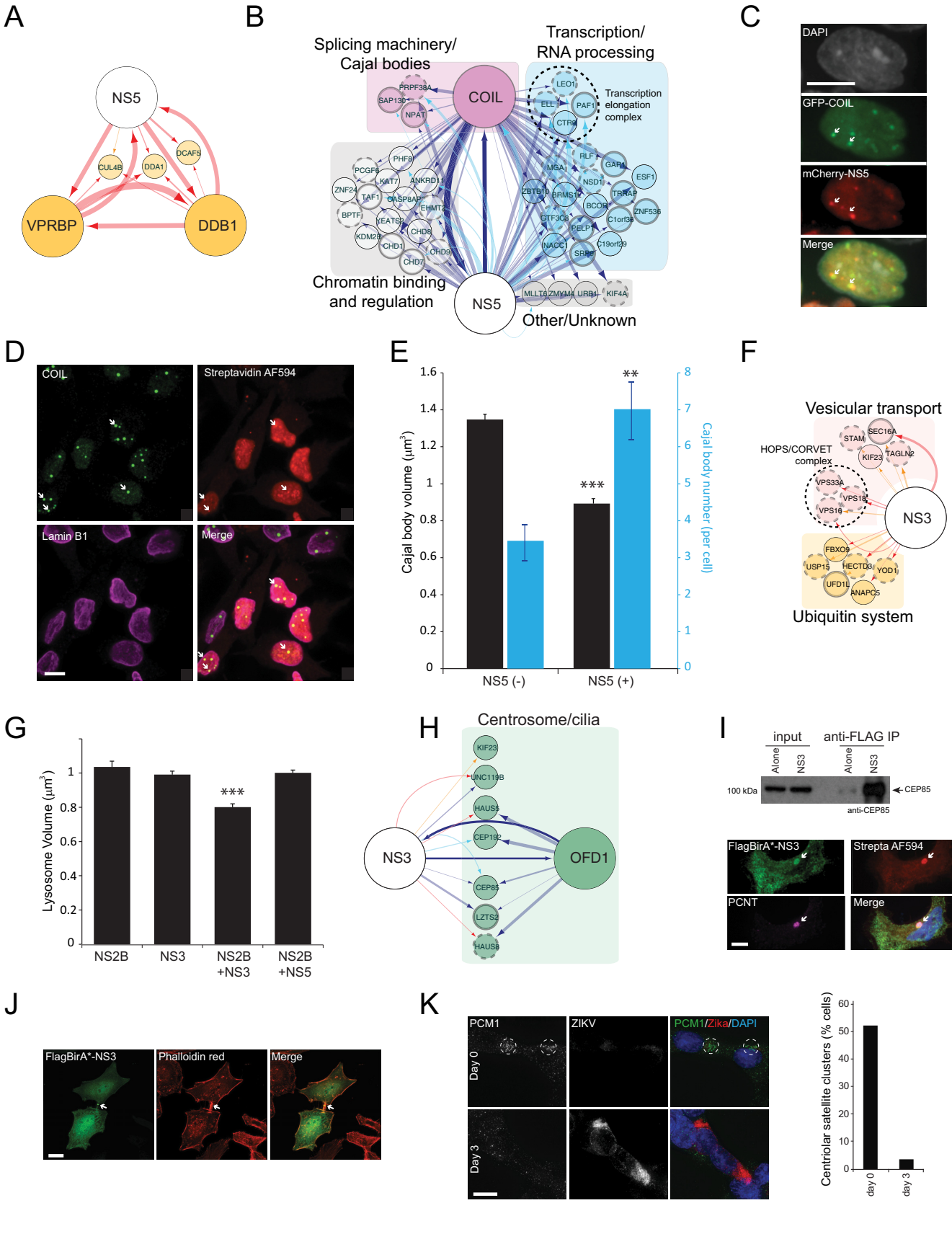
A
NS5
VPRBP
DDB1
CUL4B
DDA1
DCAF5
B
Splicing machinery/
Cajal bodies
Transcription/
RNA processing
COIL
Transcription
elongation
complex
Chromatin binding
and regulation
NS5
Other/Unknown
C
DAPI
GFP-COIL
mCherry-NS5
Merge
D
COIL
Streptavidin AF594
Lamin B1
Merge
E
Cajal body volume (μm³)
Cajal body number (per cell)
NS5 (-)
NS5 (+)
F
Vesicular transport
HOPS/CORVET
complex
NS3
Ubiquitin system
G
Lysosome Volume (μm³)
NS2B
NS3
NS2B
+NS3
NS2B
+NS5
H
Centrosome/cilia
NS3
OFD1
I
input
anti-FLAG IP
Alone
NS3
100 kDa
CEP85
anti-CEP85
FlagBirA*-NS3
Strepta AF594
PCNT
Merge
J
FlagBirA*-NS3
Phalloidin red
Merge
K
PCM1
ZIKV
PCM1/Zika/DAPI
Day 0
Day 3
Centriolar satellite clusters (% cells)
day 0
day 3

(58, 59). The NS3-OFD1 interaction was validated via BioID (Fig. 3*H*, supplemental Table S8) and the NS3-CEP85 interaction was confirmed by co-IP western (Fig. 3*I*). Consistent with these data, NS3 and its biotinylated proximity partners colocalize with pericentrin (PCNT), a component of the pericentriolar material (Fig. 3*I*). NS3 also localized to the abscission sites of dividing cells, suggesting an interaction with shared components of the centrosome and midbody (Fig. 3*J*). Although no gross defects were observed for primary cilia or centrosomes in ZIKV-infected Vero cells (data not shown), structured illumination microscopy revealed large-scale disruption of centriolar satellite clusters (Fig. 3*K*), consistent with disruption of centrosome function by ZIKV.

The peroxisome has important antiviral functions, and proteins from multiple viral classes localize to this organelle (60). Lipids synthesized exclusively in peroxisomes also appear to be required for viral replication: *e.g.* decreased peroxisome-specific ether lipid synthesis impairs influenza virus replication (61). Consistent with these studies, our data revealed extensive ZIKV protein interactions with peroxisome-associated polypeptides (Fig. 4*A*). For example, several ZIKV proteins established high confidence interactions with the peroxisomal membrane protein ABCD3/PMP70; ACBD5, VAPA and VAPB, a set of ER-peroxisome membrane contact site proteins required for lipid transfer (62, 63); and the peroxisome biogenesis protein PEX11B. ZIKV NS2A uniquely interacts with both components of the peroxisome protein import complex, PEX3 and PEX19 (Fig. 4*A*). Consistent with these data, GFP-NS2A (but no other ZIKV proteins) localizes to peroxisomes (Fig. 4*B*, supplemental Fig. S4). To begin to explore the role of the peroxisome in ZIKV biology, GFP-NS2A was expressed in a wild type (wt) human skin fibroblast cell line and fibroblast lines derived from Zellweger syndrome patients deficient for PEX19 (PBD399 (64)) or PEX3 (PBD400 (65)) and thus lacking functional peroxisomes. As expected, GFP-NS2A colocalized with peroxisomes in wt fibroblasts (Fig. 4*C*). Notably, however, it was mislocalized to the cytoplasm in both PBD399 and PBD400 cells, suggesting that NS2A is specifically targeted to peroxisomes (Fig. 4*C*).

ABCD3/PMP70 is significantly decreased in response to ZIKV infection (as compared with control proteins GAPDH and ATP5A; Fig. 4*D*). Consistent with this observation, significant decreases in peroxisome density (peroxisomes/unit cell volume) were also observed in cells expressing GFP-NS2A (Fig. 4*F*, supplemental Table S9) and in ZIKV-infected cells (Fig. 4*E*, 4*G*, supplemental Table S10). Finally, consistent with an important role for the peroxisome in ZIKV biology, ZIKV yields were significantly lower in Zellweger fibroblasts than in WT cells (Fig. 4*H*).

DISCUSSION

Together, our global ZIKV interactome identifies >1200 putative host interacting protein partners, physically linking the ten individual viral proteins to specific human polypeptides, and revealing a broad array of putative accessory functions for both the structural and nonstructural Zika polypeptides in the virus life cycle (Fig. 5; for detailed enrichment analysis, see supplemental Table S2). For example, the NS3 protease has been linked to ZIKV polyprotein cleavage and is essential for virus replication (66). Our data suggest that co-expression of NS3 and its cofactor NS2B can also impact lysosome function. Interactions between NS3 and three components of the HOPS/CORVET complex suggest that the decreased lysosome volume observed specifically in response to the coexpression of NS2B and NS3 could be because of a defect in late endosome-lysosome fusion, potentially supporting virus-containing endosome escape from lysosomal degradation and clearance. Our analysis also revealed a clear association of NS4A, NS4B and PreM with the 26S proteasome. Although these interactions remain to be investigated in an infectious context, the data suggest a putative role for this set of ZIKV proteins in *e.g.* blocking viral protein degradation, or the targeted degradation of host innate immune response proteins. As expected, C, PreM and Env were localized to the ER, where virus factories are created and viral particles assembled (67). We also detected NS2A, NS2B, NS4A, and NS4B at this organelle. These four nonstructural proteins are also likely to be involved in the formation of virus-induced membrane structures at the ER, by homology with West Nile Virus proteins (68). NS2A and NS2B are also likely to play roles in vRNA replication, as reported for the homologous proteins in the Japanese encephalitis virus (69).

The BioID approach revealed a number of associations between specific Zika polypeptides and host-cell lipid metab-

FIG. 3. **ZIKV proteins display physical and functional links with many important host cell protein complexes and multiple host organelles.** *A*, ZIKV NS5 interacts with the ubiquitin E3 ligase components DDA1, DDB1 and VPRBP/DCAF1. Reciprocal BioID conducted with both DDB1 and VPRBP/DCAF1 (in cells expressing NS5) validated these interactions. *B*, ZIKV NS5 and the Cajal Body protein coilin (COIL) share a large number of interacting partners. BioID of COIL (in cells expressing NS5) validated this interaction. *C*, NS5, and (*D*) biotinylated proteins in NS5-expressing cells, colocalize with COIL. *E*, Cells expressing NS5 display a significant decrease in average CB volume (black bars; $^{***}p < 0.001$) and an increase in the number of CB per cell (blue bars; $^{**}p < 0.01$). *F*, ZIKV NS3 interacts with host proteins linked to vesicle transport, lysosome maturation and the UPS. *G*, Lysosome volume is significantly decreased ($^{***}p < 0.001$) in cells expressing both NS3 and its cofactor NS2B. *H*, NS3 interacts with proteins linked to the centrosome and primary cilia. OFD1 BioID validates the interaction with NS3. *I*, (*top*) FlagBirA*-NS3 coIPs the endogenous CEP85 protein. (*bottom*) NS3, and biotinylated proteins in NS3-expressing cells (Strepta AF594), colocalize with the centrosome marker pericentrin (PCNT). *J*, NS3 is localized to the midbody in dividing cells. *K*, (*left*) Centriolar satellite clusters were counted at day 0 and day 3 post ZIKV-infection. ZIKV-infected Vero cells were probed with antibodies directed against the centriolar satellite marker PCM1 and ZIKV. (*right*) Cell proprtion displaying clustered centriolar satellites was quantified in uninfected and ZIKV-infected (day 3) Vero cells.

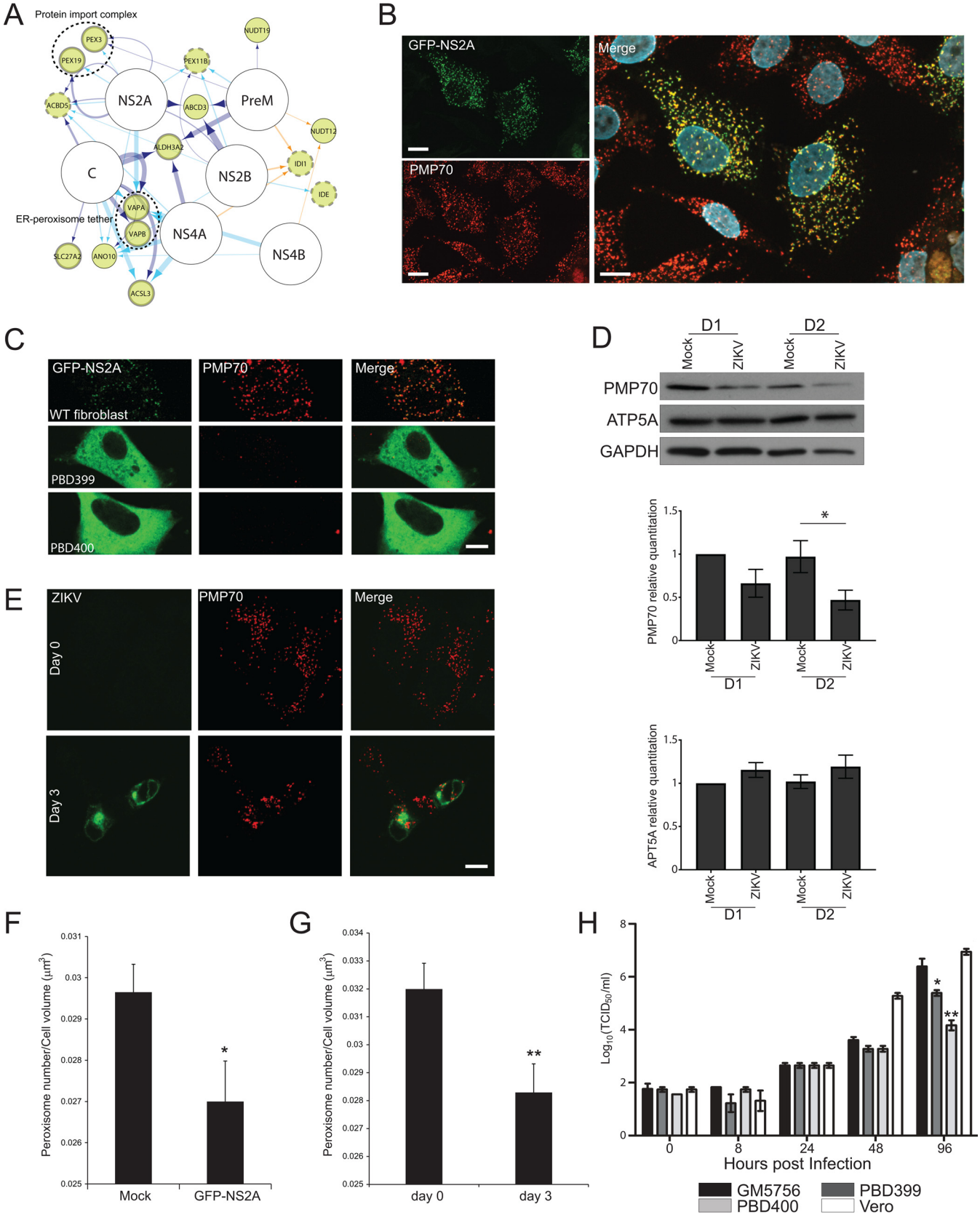
A
Protein import complex
PEX3
PEX19
NUDT19
PEX11B
NS2A
ABCD3
PreM
ACBD5
NUDT12
ALDH3A2
C
NS2B
IDI1
IDE
VAPA
ER-peroxisome tether
VAPB
NS4A
NS4B
SLC27A2
ANO10
ACSL3
B
GFP-NS2A
Merge
PMP70
C
GFP-NS2A
PMP70
Merge
WT fibroblast
PBD399
PBD400
D
D1
D2
Mock
ZIKV
Mock
ZIKV
PMP70
ATP5A
GAPDH
PMP70 relative quantitation
1.5
1
0.5
0
*
Mock
ZIKV
Mock
ZIKV
D1
D2
E
ZIKV
PMP70
Merge
Day 0
Day 3
APT5A relative quantitation
1.5
1
0.5
0
Mock
ZIKV
Mock
ZIKV
D1
D2
F
Peroxisome number/Cell volume (μm3)
0.031
0.03
0.029
0.028
0.027
0.026
0.025
*
Mock
GFP-NS2A
G
Peroxisome number/Cell volume (μm3)
0.034
0.033
0.032
0.031
0.03
0.029
0.028
0.027
0.026
0.025
**
day 0
day 3
H
Log10(TCID50/ml)
8
6
4
2
0
*
**
0
8
24
48
96
Hours post Infection
GM5756
PBD399
PBD400
Vero

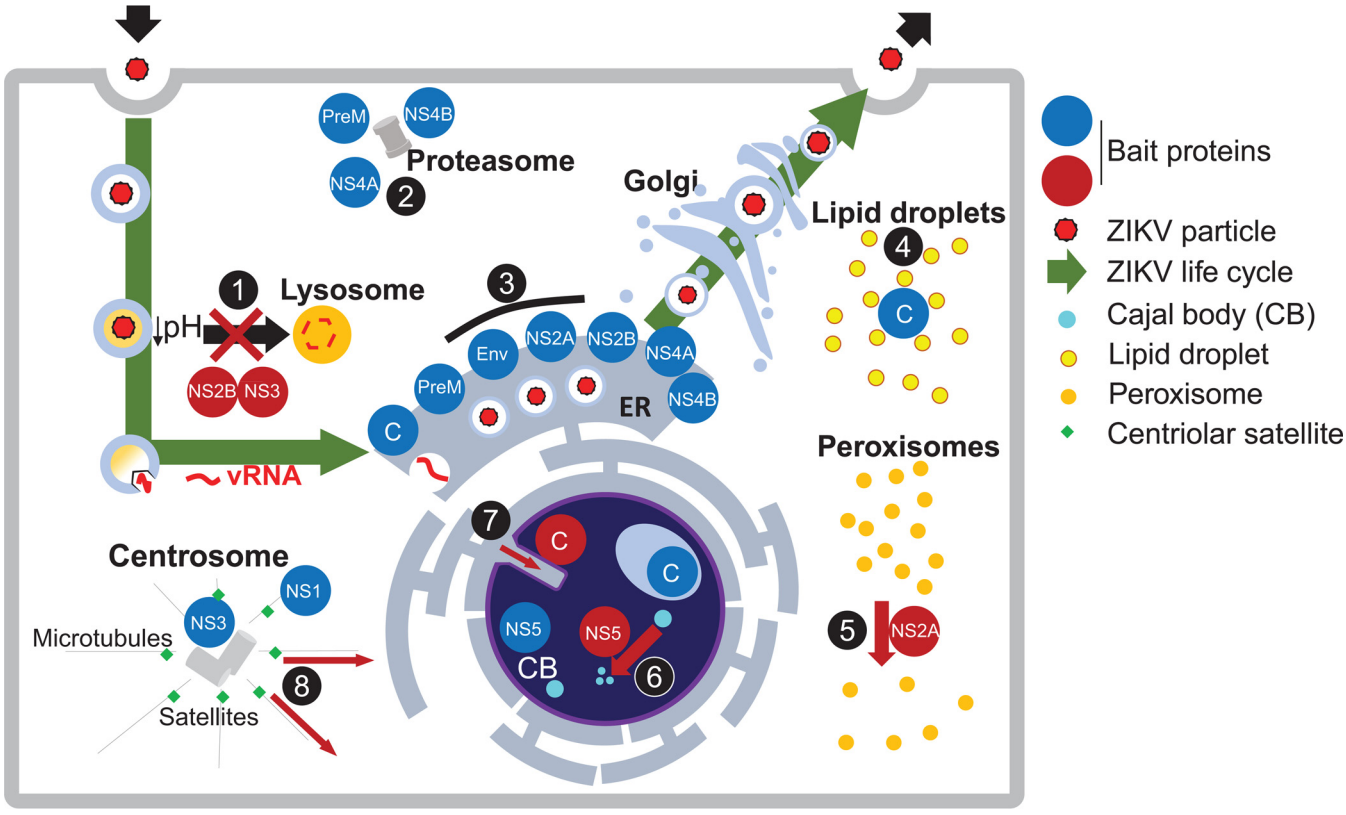

FIG. 5. **ZIKV protein localization and potential links to the ZIKV life cycle.** (1) The NS3-NS2B protease interacts with HOPS/CORVET complex components, accompanied by an apparent inhibition of late endosome-lysosome fusion. NS3-NS2B function could thus be important to protect endosomal ZIKV from lysosome-mediated degradation; (2) PreM, NS4A and NS4B are associated with the 26S proteasome. This host cell complex is commonly highjacked by viruses for *e.g.* innate immune system evasion; (3) multiple ZIKV proteins localize to the ER, consistent with roles in viral factory formation and viral replication; (4) like other Flaviviruses, the ZIKV capsid protein is addressed to lipid droplets, where it could *e.g.* highjack host-cell lipid metabolism for viral replication; (5) NS2A is uniquely localized to peroxisomes, and negatively impacts peroxisome density; (6) NS5 is localized to and appears to disrupt Cajal bodies, possibly to impair host cell splicing or usurp CB activities for viral RNA maturation; (7) ZIKV capsid protein-induced inward nuclear/ER membrane budding is likely important for the creation of viral factories; (8) Deficiencies in centrosomal proteins, including centriolar satellite components, are responsible for congenital microcephalies. ZIKV infection results in the dispersion of centriolar satellites, possibly explaining the surge in microcephaly cases associated with infected human populations.

olism machinery, which is significantly reprogrammed upon Flaviviral infection (reviewed in (70)). Like the DENV capsid polypeptide (42), the ZIKV Capsid protein was also detected at lipid droplets, where it could highjack host-cell lipid metabolism for viral replication. We also found that ZIKV NS2A is uniquely targeted to peroxisomes, an organelle that plays a critical role in lipid processing, and which acts as an important innate immune response signaling platform (60, 61). ZIKV infection or expression of NS2A alone decreased peroxisome density (organelle number/cell volume) in host cells, and ZIKV replication was significantly impaired in peroxisome-deficient cells. Together, these data suggest that NS2A targets peroxisomes to remodel host-cell lipid populations and/or to effect viral escape from the host innate immune response (as previously shown for DENV and WNV (71)).

We also detected many interactors involved in DNA and RNA metabolism. For example, ZIKV NS5 interacts with coilin, a major component of the Cajal Body (CB), a nuclear membrane-free organelle required for spliceosome maturation. We speculate that the ability of NS5 to fragment CBs could impair the processing of host-cell mRNAs, and thereby increase the availability of host ribosomes for viral RNA translation, and/or ZIKV NS5 could

FIG. 4. **Peroxisomes are required for efficient ZIKV infection.** *A*, Multiple ZIKV proteins interact with peroxisome and/or peroxisomal regulatory polypeptides. *B*, GFP-NS2A colocalizes with the peroxisome protein ABCD3/PMP70. *C*, GFP-NS2A expressed in wild type (WT) human fibroblasts localizes to peroxisomes but is mislocalized to the cytoplasm in PBD399 and PBD400 peroxisome-free cells. *D*, (*top*) Whole cell lysates from ZIKV-infected Vero cells were subjected to Western blotting, using antibodies directed against the indicated proteins. Quantitation of results (*bottom*) presented as bar graphs; $^{*}p < 0.05$. *E*, Uninfected (Day 0) and ZIKV-infected Vero cells (3d post-infection), coimmunostained for ZIKV and PMP70. *F*, Quantitation of peroxisome density (peroxisomes/cell volume) in cells expressing GFP-NS2A $^{*}p <$ 0.05 or; *G*, infected with ZIKV; $^{**}p < 0.01$. *H*, Viral titers (at indicated times post-ZIKV infection) were measured in the indicated cell lines (GM5756, wild type human fibroblasts); $^{*}p < 0.05$; $^{**}p < 0.01$.

be important for usurping CB activities required for vRNA maturation.

Notably, expression of the C protein alone induced the inward budding of nuclear/ER membranes into the nucleoplasm. The ability of C to interact with both host endomembranes and RNAs has been well documented, properties that are critical for vRNA encapsidation in Flavivirus virions (reviewed in (72)). Its positively charged carboxy-terminal domain makes it very efficient at interacting with RNAs, and we hypothesize that it could sequester host mRNAs in the nucleus to promote vRNA translation. Consistent with a previous report (73), a subpopulation of the ZIKV capsid protein is localized to the nucleolus. Capsid nucleolar localization has been documented for other Flaviviruses (74), but the function of the viral protein in this host organelle remains unclear. Addressing the capsid protein to nucleoli could be important for maintaining host ribosomal RNA production during infection, and thus preserving functional host cell translation machinery. Finally, we report that ZIKV infection is accompanied by centriolar satellite dissolution. Deficiencies in several different centrosomal proteins, including satellite components (75), have been linked to congenital microcephalies (76). Together with the specific interactions we report between ZIKV NS3 and multiple centrosome components (*e.g.* CEP192, CEP85, OFD1), this observation could help to explain the surge in microcephaly cases observed in infected human populations. The relationship between NS3 and centriolar satellites will be important to investigate.

It is important to note that the current data set: (1) does not include interactions between viral proteins; (2) describes interactions that occur under relatively high ZIKV protein expression levels, and; (3) likely lacks some virus-host protein interactions that can only be observed in the context of a viral infection. Nevertheless, our data highlight the astounding versatility of ZIKV polypeptides to simultaneously target numerous host cell organelles and provide important molecular insights into how ZIKV proteins could usurp and manipulate the host-cell machinery to the benefit of the virus. As we demonstrate here, this data set represents a rich resource that can be mined to better understand how ZIKV exploits and/or disrupts specific host cell systems and organelles, and thus paves the way for a better understanding of ZIKV biology and the identification of new antiviral targets.

Acknowledgments—We thank A. Sinha and A. Astori for outstanding technical assistance. A.-C.G. holds the Lea Reichmann chair in Cancer Proteomics and the Canada Research Chair (CRC) in Functional Proteomics.

DATA AVAILABILITY

All raw mass spectrometry data have been deposited at MassIVE (massive.ucsd.edu, accession #MSV000082311). Interaction data and all supplemental materials are available at ProHits-web.lunenfeld.ca Zika interactome project.

* Work in the A.-C.G. lab was supported by FDN143301. J.H.B. holds the Pitblado Chair in Cell Biology. B.R. holds the CRC in Proteomics and Molecular Medicine.

S This article contains supplemental material.

‡‡‡ To whom correspondence should be addressed: Princess Margaret Cancer Centre, University Health Network, Toronto, Ontario M5G 1L7, Canada. E-mail: brian.raught@uhnres.utoronto.ca.

Author contributions: E.C. conducted all ZIKV protein IP-MS and BioID work, IF confocal microscopy and MS data analysis; C.R. performed ZIKV infections and $TCID_{50}$ measurements; D.C. conducted peroxisome staining and quantitation; J.G. performed centrosome protein pulldowns, SIM microscopy and satellite data analysis, BJAD generated FlagBirA-coilin expressing cells and conducted coilin BioID; E.M.N.L. cloned all ZIKV bait expression constructs and assisted with cell culture and MS sample preparation; J.S.-G. performed MS acquisition and data migration; A.-C.G., J.H.B., P.K.K., D.S., and B.R. directed the project. E.C. and B.R. wrote the manuscript.

REFERENCES

1. Petersen, L. R., Jamieson, D. J., Powers, A. M., and Honein, M. A. (2016) Zika Virus. *N. Engl. J. Med.* **374,** 1552–1563
2. Chen, H. L., and Tang, R. B. (2016) Why Zika virus infection has become a public health concern? *J. Chin. Med. Assoc.* **79,** 174–178
3. Dick, G. W., Kitchen, S. F., and Haddow, A. J. (1952) Zika virus. I. Isolations and serological specificity. *Trans. R. Soc. Trop. Med. Hyg.* **46,** 509–520
4. Duffy, M. R., Chen, T. H., Hancock, W. T., Powers, A. M., Kool, J. L., Lanciotti, R. S., Pretrick, M., Marfel, M., Holzbauer, S., Dubray, C., Guillaumot, L., Griggs, A., Bel, M., Lambert, A. J., Laven, J., Kosoy, O., Panella, A., Biggerstaff, B. J., Fischer, M., and Hayes, E. B. (2009) Zika virus outbreak on Yap Island, Federated States of Micronesia. *N. Engl. J. Med.* **360,** 2536–2543
5. Cao-Lormeau, V. M., Roche, C., Teissier, A., Robin, E., Berry, A. L., Mallet, H. P., Sall, A. A., and Musso, D. (2014) Zika virus, French polynesia, South pacific, 2013. *Emerg. Infect. Dis.* **20,** 1085–1086
6. Zanluca, C., Melo, V. C., Mosimann, A. L., Santos, G. I., Santos, C. N., and Luz, K. (2015) First report of autochthonous transmission of Zika virus in Brazil. *Mem. Inst. Oswaldo Cruz* **110,** 569–572
7. Campos, G. S., Bandeira, A. C., and Sardi, S. I. (2015) Zika Virus Outbreak, Bahia, Brazil. *Emerg. Infect. Dis.* **21,** 1885–1886
8. Poland, G. A., Kennedy, R. B., Ovsyannikova, I. G., Palacios, R., Ho, P. L., and Kalil, J. (2018) Development of vaccines against Zika virus. *Lancet Infect Dis.* **18,** e211–e219
9. Tang, H., Hammack, C., Ogden, S. C., Wen, Z., Qian, X., Li, Y., Yao, B., Shin, J., Zhang, F., Lee, E. M., Christian, K. M., Didier, R. A., Jin, P., Song, H., and Ming, G. L. (2016) Zika virus infects human cortical neural progenitors and attenuates their growth. *Cell Stem Cell* **18,** 587–590
10. Lin, M. Y., Wang, Y. L., Wu, W. L., Wolseley, V., Tsai, M. T., Radic, V., Thornton, M. E., Grubbs, B. H., Chow, R. H., and Huang, I. C. (2017) Zika virus infects intermediate progenitor cells and post-mitotic committed neurons in human fetal brain tissues. *Sci. Rep.* **7,** 14883
11. Gatherer, D., and Kohl, A. (2016) Zika virus: a previously slow pandemic spreads rapidly through the Americas. *J. Gen. Virol.* **97,** 269–273
12. Blazquez, A. B., and Saiz, J. C. (2016) Neurological manifestations of Zika virus infection. *World J. Virol.* **5,** 135–143
13. Li, C., Xu, D., Ye, Q., Hong, S., Jiang, Y., Liu, X., Zhang, N., Shi, L., Qin, C. F., and Xu, Z. (2016) Zika virus disrupts neural progenitor development and leads to microcephaly in mice. *Cell Stem Cell* **19,** 120–126
14. Devhare, P., Meyer, K., Steele, R., Ray, R. B., and Ray, R. (2017) Zika virus infection dysregulates human neural stem cell growth and inhibits differentiation into neuroprogenitor cells. *Cell Death Dis.* **8,** e3106
15. Mlakar, J., Korva, M., Tul, N., Popovic, M., Poljsak-Prijatelj, M., Mraz, J., Kolenc, M., Resman Rus, K., Vesnaver Vipotnik, T., Fabjan Vodusek, V., Vizjak, A., Pizem, J., Petrovec, M., and Avsic Zupanc, T. (2016) Zika virus associated with microcephaly. *N. Engl. J. Med.* **374,** 951–958
16. Merfeld, E., Ben-Avi, L., Kennon, M., and Cerveny, K. L. (2017) Potential mechanisms of Zika-linked microcephaly. *Wiley Interdiscip. Rev. Dev. Biol.* **6**, e273
17. Perera-Lecoin, M., Meertens, L., Carnec, X., and Amara, A. (2013) Flavivirus entry receptors: an update. *Viruses* **6,** 69–88

18. Kuno, G., and Chang, G. J. (2007) Full-length sequencing and genomic characterization of Bagaza, Kedougou, and Zika viruses. *Arch. Virol.* **152,** 687–696
19. Shankar, A., Patil, A. A., and Skariyachan, S. (2017) Recent perspectives on genome, transmission, clinical manifestation, diagnosis, therapeutic strategies, vaccine developments, and challenges of Zika virus research. *Front. Microbiol.* **8,** 1761
20. Wang, A., Thurmond, S., Islas, L., Hui, K., and Hai, R. (2017) Zika virus genome biology and molecular pathogenesis. *Emerg. Microbes Infect.* **6,** e13
21. Savidis, G., McDougall, W. M., Meraner, P., Perreira, J. M., Portmann, J. M., Trincucci, G., John, S. P., Aker, A. M., Renzette, N., Robbins, D. R., Guo, Z., Green, S., Kowalik, T. F., and Brass, A. L. (2016) Identification of Zika virus and Dengue virus dependency factors using functional genomics. *Cell Rep.* **16,** 232–246
22. Marceau, C. D., Puschnik, A. S., Majzoub, K., Ooi, Y. S., Brewer, S. M., Fuchs, G., Swaminathan, K., Mata, M. A., Elias, J. E., Sarnow, P., and Carette, J. E. (2016) Genetic dissection of Flaviviridae host factors through genome-scale CRISPR screens. *Nature* **535,** 159–163
23. Yasunaga, A., Hanna, S. L., Li, J., Cho, H., Rose, P. P., Spiridigliozzi, A., Gold, B., Diamond, M. S., and Cherry, S. (2014) Genome-wide RNAi screen identifies broadly-acting host factors that inhibit arbovirus infection. *PLoS Pathog.* **10,** e1003914
24. Coyaud, E., Mis, M., Laurent, E. M., Dunham, W. H., Couzens, A. L., Robitaille, M., Gingras, A. C., Angers, S., and Raught, B. (2015) BioID-based identification of Skp Cullin F-box (SCF)beta-TrCP1/2 E3 ligase substrates. *Mol. Cell. Proteomics* **14,** 1781–1795
25. Kessner, D., Chambers, M., Burke, R., Agus, D., and Mallick, P. (2008) ProteoWizard: open source software for rapid proteomics tools development. *Bioinformatics* **24,** 2534–2536
26. Craig, R., and Beavis, R. C. (2004) TANDEM: matching proteins with tandem mass spectra. *Bioinformatics* **20,** 1466–1467
27. Eng, J. K., Jahan, T. A., and Hoopmann, M. R. (2013) Comet: an open-source MS/MS sequence database search tool. *Proteomics* **13,** 22–24
28. Baronti, C., Piorkowski, G., Charrel, R. N., Boubis, L., Leparc-Goffart, I., and de Lamballerie, X. (2014) Complete coding sequence of zika virus from a French polynesia outbreak in 2013. *Genome Announc.* **2,** e00500-14
29. Shaw, G., Morse, S., Ararat, M., and Graham, F. L. (2002) Preferential transformation of human neuronal cells by human adenoviruses and the origin of HEK 293 cells. *Faseb J* **16,** 869–871
30. Monel, B., Compton, A. A., Bruel, T., Amraoui, S., Burlaud-Gaillard, J., Roy, N., Guivel-Benhassine, F., Porrot, F., Genin, P., Meertens, L., Sinigaglia, L., Jouvenet, N., Weil, R., Casartelli, N., Demangel, C., Simon-Loriere, E., Moris, A., Roingeard, P., Amara, A., and Schwartz, O. (2017) Zika virus induces massive cytoplasmic vacuolization and paraptosis-like death in infected cells. *EMBO J.* **36,** 1653–1668
31. Roux, K. J., Kim, D. I., Raida, M., and Burke, B. (2012) A promiscuous biotin ligase fusion protein identifies proximal and interacting proteins in mammalian cells. *J. Cell Biol.* **196,** 801–810
32. Uhlen, M., Oksvold, P., Fagerberg, L., Lundberg, E., Jonasson, K., Forsberg, M., Zwahlen, M., Kampf, C., Wester, K., Hober, S., Wernerus, H., Bjorling, L., and Ponten, F. (2010) Towards a knowledge-based Human Protein Atlas. *Nat. Biotechnol.* **28,** 1248–1250
33. Lambert, J. P., Tucholska, M., Go, C., Knight, J. D., and Gingras, A. C. (2015) Proximity biotinylation and affinity purification are complementary approaches for the interactome mapping of chromatin-associated protein complexes. *J. Proteomics* **118,** 81–94
34. Gupta, G. D., Coyaud, E., Goncalves, J., Mojarad, B. A., Liu, Y., Wu, Q., Gheiratmand, L., Comartin, D., Tkach, J. M., Cheung, S. W., Bashkurov, M., Hasegan, M., Knight, J. D., Lin, Z. Y., Schueler, M., Hildebrandt, F., Moffat, J., Gingras, A. C., Raught, B., and Pelletier, L. (2015) A dynamic protein interaction landscape of the human centrosome-cilium interface. *Cell* **163,** 1484–1499
35. Ma, H., Dang, Y., Wu, Y., Jia, G., Anaya, E., Zhang, J., Abraham, S., Choi, J. G., Shi, G., Qi, L., Manjunath, N., and Wu, H. (2015) A CRISPR-based screen identifies genes essential for West-Nile-virus-induced cell death. *Cell Rep.* **12,** 673–683
36. Zhang, R., Miner, J. J., Gorman, M. J., Rausch, K., Ramage, H., White, J. P., Zuiani, A., Zhang, P., Fernandez, E., Zhang, Q., Dowd, K. A., Pierson, T. C., Cherry, S., and Diamond, M. S. (2016) A CRISPR screen defines a signal peptide processing pathway required by flaviviruses. *Nature* **535,** 164–168
37. Balinsky, C. A., Schmeisser, H., Ganesan, S., Singh, K., Pierson, T. C., and Zoon, K. C. (2013) Nucleolin interacts with the dengue virus capsid protein and plays a role in formation of infectious virus particles. *J. Virol.* **87,** 13094–13106
38. Khaminets, A., Heinrich, T., Mari, M., Grumati, P., Huebner, A. K., Akutsu, M., Liebmann, L., Stolz, A., Nietzsche, S., Koch, N., Mauthe, M., Katona, I., Qualmann, B., Weis, J., Reggiori, F., Kurth, I., Hubner, C. A., and Dikic, I. (2015) Regulation of endoplasmic reticulum turnover by selective autophagy. *Nature* **522,** 354–358
39. Lennemann, N. J., and Coyne, C. B. (2017) Dengue and Zika viruses subvert reticulophagy by NS2B3-mediated cleavage of FAM134B. *Autophagy*, **13**, 322–332
40. Bell, T. M., Field, E. J., and Narang, H. K. (1971) Zika virus infection of the central nervous system of mice. *Arch Gesamte Virusforsch* **35,** 183–193
41. Rossignol, E. D., Peters, K. N., Connor, J. H., and Bullitt, E. (2017) Zika virus induced cellular remodeling. *Cell Microbiol.* **19,** e12740
42. Samsa, M. M., Mondotte, J. A., Iglesias, N. G., Assuncao-Miranda, I., Barbosa-Lima, G., Da Poian, A. T., Bozza, P. T., and Gamarnik, A. V. (2009) Dengue virus capsid protein usurps lipid droplets for viral particle formation. *PLoS Pathog.* **5,** e1000632
43. Grant, A., Ponia, S. S., Tripathi, S., Balasubramaniam, V., Miorin, L., Sourisseau, M., Schwarz, M. C., Sanchez-Seco, M. P., Evans, M. J., Best, S. M., and Garcia-Sastre, A. (2016) Zika virus targets human STAT2 to inhibit type I interferon signaling. *Cell Host Microbe* **19,** 882–890
44. Barry, M., and Fruh, K. (2006) Viral modulators of cullin RING ubiquitin ligases: culling the host defense. *Sci STKE* **2006,** pe21
45. Machyna, M., Heyn, P., and Neugebauer, K. M. (2013) Cajal bodies: where form meets function. *Wiley Interdiscip. Rev. RNA* **4,** 17–34
46. Hofer, C. T., Jolmes, F., Haralampiev, I., Veit, M., and Herrmann, A. (2016) Influenza A virus nucleoprotein targets subnuclear structures. *Cell Microbiol.***19,** e12679
47. Sivan, G., Ormanoglu, P., Buehler, E. C., Martin, S. E., and Moss, B. (2015) Identification of restriction factors by human genome-wide RNA interference screening of viral host range mutants exemplified by discovery of SAMD9 and WDR6 as inhibitors of the Vaccinia virus K1L-C7L- mutant. *MBio* **6,** e01122
48. Cleret-Buhot, A., Zhang, Y., Planas, D., Goulet, J. P., Monteiro, P., Gosselin, A., Wacleche, V. S., Tremblay, C. L., Jenabian, M. A., Routy, J. P., El-Far, M., Chomont, N., Haddad, E. K., Sekaly, R. P., and Ancuta, P. (2015) Identification of novel HIV-1 dependency factors in primary CCR4(+)CCR6(+)Th17 cells via a genome-wide transcriptional approach. *Retrovirology* **12,** 102
49. Sessions, O. M., Barrows, N. J., Souza-Neto, J. A., Robinson, T. J., Hershey, C. L., Rodgers, M. A., Ramirez, J. L., Dimopoulos, G., Yang, P. L., Pearson, J. L., and Garcia-Blanco, M. A. (2009) Discovery of insect and human dengue virus host factors. *Nature* **458,** 1047–1050
50. Krishnan, M. N., Ng, A., Sukumaran, B., Gilfoy, F. D., Uchil, P. D., Sultana, H., Brass, A. L., Adametz, R., Tsui, M., Qian, F., Montgomery, R. R., Lev, S., Mason, P. W., Koski, R. A., Elledge, S. J., Xavier, R. J., Agaisse, H., and Fikrig, E. (2008) RNA interference screen for human genes associated with West Nile virus infection. *Nature* **455,** 242–245
51. Balderhaar, H. J., and Ungermann, C. (2013) CORVET and HOPS tethering complexes - coordinators of endosome and lysosome fusion. *J. Cell Sci.* **126,** 1307–1316
52. Carette, J. E., Raaben, M., Wong, A. C., Herbert, A. S., Obernosterer, G., Mulherkar, N., Kuehne, A. I., Kranzusch, P. J., Griffin, A. M., Ruthel, G., Dal Cin, P., Dye, J. M., Whelan, S. P., Chandran, K., and Brummelkamp, T. R. (2011) Ebola virus entry requires the cholesterol transporter Niemann-Pick C1. *Nature* **477,** 340–343
53. Lei, J., Hansen, G., Nitsche, C., Klein, C. D., Zhang, L., and Hilgenfeld, R. (2016) Crystal structure of Zika virus NS2B-NS3 protease in complex with a boronate inhibitor. *Science* **353,** 503–505
54. Gabriel, E., Ramani, A., Karow, U., Gottardo, M., Natarajan, K., Gooi, L. M., Goranci-Buzhala, G., Krut, O., Peters, F., Nikolic, M., Kuivanen, S., Korhonen, E., Smura, T., Vapalahti, O., Papantonis, A., Schmidt-Chanasit, J., Riparbelli, M., Callaini, G., Kronke, M., Utermohlen, O., and Gopalakrishnan, J. (2017) Recent Zika virus isolates induce premature differentiation of neural progenitors in human brain organoids. *Cell Stem Cell* **20,** 397–406.e5

55. Wolf, B., Diop, F., Ferraris, P., Wichit, S., Busso, C., Misse, D., and Gonczy, P. (2017) Zika virus causes supernumerary foci with centriolar proteins and impaired spindle positioning. *Open Biol* **7,** 160231
56. Zhang, Q., Li, Y., Zhang, Y., Torres, V. E., Harris, P. C., Ling, K., and Hu, J. (2016) GTP-binding of ARL-3 is activated by ARL-13 as a GEF and stabilized by UNC-119. *Sci Rep.* **6,** 24534
57. Macca, M., and Franco, B. (2009) The molecular basis of oral-facial-digital syndrome, type 1. *Am. J. Med. Genet. C Semin. Med. Genet.* **151C,** 318–325
58. Tsuchiya, Y., Yoshiba, S., Gupta, A., Watanabe, K., and Kitagawa, D. (2016) Cep295 is a conserved scaffold protein required for generation of a bona fide mother centriole. *Nat. Commun.* **7,** 12567
59. Chen, C., Tian, F., Lu, L., Wang, Y., Xiao, Z., Yu, C., and Yu, X. (2015) Characterization of Cep85 - a new antagonist of Nek2A that is involved in the regulation of centrosome disjunction. *J. Cell Sci.* **128,** 3290–3303
60. Odendall, C., and Kagan, J. C. (2013) Peroxisomes and the antiviral responses of mammalian cells. *Subcell. Biochem.* **69,** 67–75
61. Tanner, L. B., Chng, C., Guan, X. L., Lei, Z., Rozen, S. G., and Wenk, M. R. (2014) Lipidomics identifies a requirement for peroxisomal function during influenza virus replication. *J. Lipid Res.* **55,** 1357–1365
62. Hua, R., Cheng, D., Freeman, S., Di Pietro, E., Coyaud, E., Wang, Y., Vissa, A., Demers, N., Yip, C. M., Fairn, G. D., Braverman, N., Brumell, J., Trimble, W., Raught, B., and Kim, P. K. (2017) VAPs and ACBD5 tether peroxisomes to the ER for peroxisome maintenance and lipid homeostasis. *J. Cell Biol.* **216,** 367–377
63. Costello, J. L., Castro, I. G., Hacker, C., Schrader, T. A., Metz, J., Zeuschner, D., Azadi, A. S., Godinho, L. F., Costina, V., Findeisen, P., Manner, A., Islinger, M., and Schrader, M. (2017) ACBD5 and VAPB mediate membrane associations between peroxisomes and the ER. *J. Cell Biol.* **216,** 331–342
64. Sacksteder, K. A., Jones, J. M., South, S. T., Li, X., Liu, Y., and Gould, S. J. (2000) PEX19 binds multiple peroxisomal membrane proteins, is predominantly cytoplasmic, and is required for peroxisome membrane synthesis. *J. Cell Biol.* **148,** 931–944
65. South, S. T., Sacksteder, K. A., Li, X., Liu, Y., and Gould, S. J. (2000) Inhibitors of COPI and COPII do not block PEX3-mediated peroxisome synthesis. *J. Cell Biol.* **149,** 1345–1360
66. Luo, D., Vasudevan, S. G., and Lescar, J. (2015) The flavivirus NS2B-NS3 protease-helicase as a target for antiviral drug development. *Antiviral Res.* **118,** 148–158
67. Blazevic, J., Rouha, H., Bradt, V., Heinz, F. X., and Stiasny, K. (2016) Membrane anchors of the structural flavivirus proteins and their role in virus assembly. *J. Virol.* **90,** 6365–6378
68. Kaufusi, P. H., Kelley, J. F., Yanagihara, R., and Nerurkar, V. R. (2014) Induction of endoplasmic reticulum-derived replication-competent membrane structures by West Nile virus non-structural protein 4B. *PLoS ONE* **9,** e84040
69. Li, X. D., Deng, C. L., Ye, H. Q., Zhang, H. L., Zhang, Q. Y., Chen, D. D., Zhang, P. T., Shi, P. Y., Yuan, Z. M., and Zhang, B. (2016) Transmembrane domains of NS2B contribute to both viral RNA replication and particle formation in Japanese encephalitis virus. *J. Virol.* **90,** 5735–5749
70. Martin-Acebes, M. A., Vazquez-Calvo, A., and Saiz, J. C. (2016) Lipids and flaviviruses, present and future perspectives for the control of dengue, Zika, and West Nile viruses. *Prog. Lipid Res.* **64,** 123–137
71. You, J., Hou, S., Malik-Soni, N., Xu, Z., Kumar, A., Rachubinski, R. A., Frappier, L., and Hobman, T. C. (2015) Flavivirus infection impairs peroxisome biogenesis and early antiviral signaling. *J. Virol.* **89,** 12349–12361
72. Oliveira, E. R. A., Mohana-Borges, R., de Alencastro, R. B., and Horta, B. A. C. (2017) The flavivirus capsid protein: Structure, function and perspectives towards drug design. *Virus Res.* **227,** 115–123
73. Hou, W., Cruz-Cosme, R., Armstrong, N., Obwolo, L. A., Wen, F., Hu, W., Luo, M. H., and Tang, Q. (2017) Molecular cloning and characterization of the genes encoding the proteins of Zika virus. *Gene* **628,** 117–128
74. Wang, S. H., Syu, W. J., Huang, K. J., Lei, H. Y., Yao, C. W., King, C. C., and Hu, S. T. (2002) Intracellular localization and determination of a nuclear localization signal of the core protein of dengue virus. *J. Gen. Virol.* **83,** 3093–3102
75. Kodani, A., Yu, T. W., Johnson, J. R., Jayaraman, D., Johnson, T. L., Al-Gazali, L., Sztriha, L., Partlow, J. N., Kim, H., Krup, A. L., Dammermann, A., Krogan, N. J., Walsh, C. A., and Reiter, J. F. (2015) Centriolar satellites assemble centrosomal microcephaly proteins to recruit CDK2 and promote centriole duplication. *Elife* **4,** e07519
76. Chavali, P. L., Putz, M., and Gergely, F. (2014) Small organelle, big responsibility: the role of centrosomes in development and disease. *Philos. Trans. R. Soc. Lond. B Biol. Sci.* **369,** 20130468